



## Boiling characteristics on the reduced graphene oxide films



Ho Seon Ahn<sup>a</sup>, Ji Min Kim<sup>b</sup>, Jin Man Kim<sup>c</sup>, Su Cheong Park<sup>b</sup>, Kyungwon Hwang<sup>b</sup>, Hang Jin Jo<sup>c</sup>,  
Taejoo Kim<sup>d</sup>, Dong Wook Jerng<sup>e</sup>, Massoud Kaviany<sup>f</sup>, Moo Hwan Kim<sup>c,\*</sup>

<sup>a</sup> Division of Mechanical System Engineering, Incheon National University, Incheon, Republic of Korea

<sup>b</sup> Department of Mechanical Engineering, POSTECH, Pohang, Republic of Korea

<sup>c</sup> Division of Advanced Nuclear Engineering, POSTECH, Pohang, Republic of Korea

<sup>d</sup> Korea Atomic Energy Research Institute, Daejeon, Republic of Korea

<sup>e</sup> School of Energy Systems Engineering, Chung-Ang University, Seoul, Republic of Korea

<sup>f</sup> Department of Mechanical Engineering, University of Michigan, Ann Arbor, USA

### ARTICLE INFO

#### Article history:

Received 15 November 2013

Received in revised form 7 May 2014

Accepted 15 May 2014

Available online 2 June 2014

#### Keywords:

Pool boiling

Critical heat flux

Reduced graphene oxide

### ABSTRACT

The graphene has been interested world-widely for the superb mechanical and electrical properties. Among them, the thermal conductivity of graphene was often reported as the 500–5000 W/mK. We tried to apply the graphene to the thermal application of boiling heat transfer through the graphene coating. The graphene was used for the reduced graphene oxide flakes in water (RGO colloid). The RGO colloid boiling on silicon-dioxide heater (substrate) showed both the boiling heat transfer and the critical heat flux enhancement as 65% and 70%, respectively. After RGO colloid boiling, the base graphene layer (BGL) with 10–100 nm thickness below the self-assembled foam-like graphene (SFG) was observed. In order to confirm the effect of BGL on the enhanced boiling performance, the only water boiling on an artificial graphene multilayers (RGO film) coated heater was conducted, and shows the similar result with the RGO colloid boiling.

© 2014 Elsevier Inc. All rights reserved.

## 1. Introduction

Boiling heat transfer (liquid–vapor phase change) include the several applications such as a nuclear power plant energy transfer, electronic chip cooling, and various chemical processes, because of the most efficient heat transfer performance. During boiling heat transfer, the two critical issues are performance (boiling heat transfer coefficient) and critical heat flux (CHF), which is the limit of boiling heat transfer in a thermal system. Thus, thermal systems of this type require enhanced boiling heat transfer (BHT) and increased CHF. Over the past century, numerous techniques for providing high BHT and CHF have been developed. Recently, since the nanofluids boiling provided the nano and microscaled structures on the heating surface, there has been a lot studies for CHF enhancement mechanism in nanofluids; representative factors of CHF enhancement are the improved surface wettability and the capillary wicking. [1–5] However, among CHF enhancement in nanofluids, there was a critical problem such as the degradation of BHT, because of the reduction of active nucleate sites and the

low performance of bubble dynamics. [6,7] Most recently, a number of researchers have investigated ways of increasing both BHT and CHF in nanofluids. Kwark et al. [8] reported that the BHT coefficient and CHF could be increased simultaneously by controlling the thickness of the nanoparticle coating layer. They have controlled the heat flux and the coating time as the coating parameters. However, it seems to need the further studies of both increasing the CHF and the boiling heat transfer.

Graphene has gained much attention recently due to its high thermal conductivity ( $900\text{--}5000\text{ W K}^{-1}\text{ m}^{-1}$ ) [9], high transparency [10], ultra-high electric conductivity [11], and novel mechanical properties [12]. However, little information about the thermal characteristics or applications of graphene is available. Since graphene exists as ultra-thin and microscale flakes, considerable effort has been made to synthesize large-area films that retain the superb properties of graphene. Among them, soluble graphene in water solvent has been highlighted through the oxidation process of graphene. Through a chemical process with hydrazine, graphene oxide (GO) can be changed to a reduced graphene oxide (RGO), which can have properties similar to graphene. [13] Jang et al. [14] estimated the thermal conductivity of RGO film to be  $110\text{--}1100\text{ W K}^{-1}\text{ m}^{-1}$  at room temperature. They found that the measured thermal conductivity of an RGO film on a silicon

\* Corresponding author. Address: Korea Institute of Nuclear Safety (KINS), Daejeon, Republic of Korea.

E-mail address: [mhkim@postech.ac.kr](mailto:mhkim@postech.ac.kr) (M.H. Kim).

substrate increased as the film grew thicker (from 110 to  $1100 \text{ W K}^{-1} \text{ m}^{-1}$  when its thickness increased from 1 to 100 nm at room temperature). Even though the thermal conductivity of a graphene film is much lower than that of graphene flakes, it is still higher than that of other substrates, and hence graphene remains attractive for thermal applications.

In this paper, we investigated the effect of RGO as the heater surface and the working fluids for the pool boiling characteristics. First, the RGO films with sub-micrometer thickness were prepared by the filtration process and the transfer method (from membrane filter to heater surface). Second, the RGO colloid as the working fluid was prepared directly, which the RGO flakes were well-dispersed in DI water. Through the experiments of pool boiling with CHF tests, we reports the roles of RGO as a heater and a working fluid to enhance the boiling heat transfer and the critical heat flux.

## 2. Experiments

### 2.1. Experimental pool boiling facility

Fig. 1 shows a diagram of the experimental pool boiling facility, which was designed to carry out pool boiling experiments for BHT and CHF under atmospheric pressure via the electrical Joule heating method. It was composed of a test sample and a main pool chamber. The test sample consisted of a silicon dioxide heater ( $\text{SiO}_2$  surface) and a polyetheretherketone (PEEK) test sample frame. PEEK is a thermoplastic that has high thermal resistance, and is compatible with an aqueous/chemical environment. The test samples were waterproofed with adhesive sealant (Permatex clear room-temperature vulcanizing (RTV) silicone) and fixed with binary epoxy (Duralco 4461). The main pool chamber was a rectangular assembled bath made of 10-mm aluminum plate with a 4-l capacity. The test sample was placed on the bottom of the pool chamber. A reflux condenser was installed at the top of the main pool chamber to prevent evaporation of the water.

### 2.2. Test heater and data acquisition

Fig. 2 shows images of the test heater used in the present work, consisting of double-polished silicon dioxide ( $\text{SiO}_2$ ) backed with a platinum thin-film heater. The test heater was composed of rectangular silicon wafer plate. The silicon substrate measured  $25 \times 20 \text{ mm}$ , and had a  $\text{SiO}_2$  layer to eliminate native oxidation

effects on both the top and bottom surfaces. The heating element was a platinum thin film with a thickness of 1200 Å, layered onto the bottom of the substrate using an electron-beam (E-beam) evaporator. A titanium thin film with a thickness of 120 Å was used for the adhesion layer between the silicon wafer and the platinum film. The complete platinum film heater was H-shaped ( $15 \times 10 \text{ mm}$ ), and was the main heating area. Wire electrodes were attached by lead soldering, so that the resistance of the electrodes was less than 1% of the total sample resistance. The Joule heating method uses electrical power to heat samples directly via conductor resistance. For the purpose of calibrating the wall temperature, it is important to know the exact voltage and current during actual operation, so that the resistance of each test sample can be correlated as a function of temperature (calibration chart), as shown in Fig. 3. A direct current (DC) power supply (120 V/18 A) was used to provide power to the Joule heating system. The voltage applied to the test sample was measured directly, using a power measuring line and data acquisition system with a 1-s period. The reference resistance unit (Vishay, RH02510R00FC02) was immersed in a constant-temperature bath at  $10^\circ \text{C}$ , and used to calculate the exact current passing through the test sample. The heat flux ( $q''$ ) was estimated from the voltage applied to the test heater ( $V_{\text{heater}}$ ), the reference resistor voltage load ( $I_{\text{circuit}} = V_{\text{ref}}/R_{\text{ref}}$ , where  $V_{\text{ref}}$  and  $R_{\text{ref}}$  denote the voltage load on the reference resistance unit and the constant reference resistance, respectively), and the heating area ( $A_{\text{heater}}$ ) as follows:

$$q'' = \frac{V_{\text{heater}} I_{\text{circuit}}}{A_{\text{heater}}} \quad (1)$$

The wall temperature was estimated from the calibration chart for each sample, using the measured resistance of the test heater ( $R_{\text{heater}} = V_{\text{heater}}/I_{\text{circuit}}$ ). The uncertainty of test heater was evaluated by Holman's guide [15] (see Appendix A). In addition, we tried to consider the effect of heat spreading (lateral conduction due to the difference of size between the actual heating area ( $10 \times 15 \text{ mm}$ ) and the surface area ( $25 \times 20 \text{ mm}$ )). To include the effect of heat spreading and heat loss from backside PT heater, the numerical simulation was conducted as COMSOL 4.0 and Matlab 7.0 in our previous study. [16] Based on measured bottom heat flux and temperature information, the reduction procedure is progressed with several heat transfer coefficients till the calculated values match the experimental magnitude. When one used heat transfer coefficient for numerical simulation satisfy experimentally obtained target condition's magnitude, we determined on these heat transfer coefficients as our result for the evaluation of heat loss amount. Finally, the heat loss was 6.7–21% regarding to the applied heat flux, however, the comparison with boiling performance and critical heat flux could be reasonable.

### 2.3. Preparation of the RGO colloid

The procedure for the synthesis of the RGO flakes was as follows. A mixture of 55 mg of GO in 55 mL of water was ultra-sonicated in a high-intensity ultrasonic processor (Autotune Series, 750 W) for 30 min. The solution was then centrifuged (MF500 centrifuge, Hanil) at 3000 rpm for 30 min. Next, 50 mL of the GO solution was diluted with 50 mL of distilled water containing 50  $\mu\text{L}$  of hydrazine solution (35 wt.%, Aldrich) and 250  $\mu\text{L}$  of ammonia solution ( $\sim 30\%$ ). After a few minutes of vigorous mixing, the solution was maintained at  $95^\circ \text{C}$  for 3 h [17]. The solubility of RGO is approximately 0.3 mg/mL. The amount of RGO in the solution was measured by filtering a known amount of the solution and weighing the RGO and filter paper. A photograph of the RGO flakes suspended in deionized water is shown in Fig. 3(a). A transmission electron microscopy (TEM) image of typical RGO flakes synthesized by the above method is shown in Fig. 3(b). The inset image of Fig. 3(b) shows the selected-area electron diffraction (SAED)

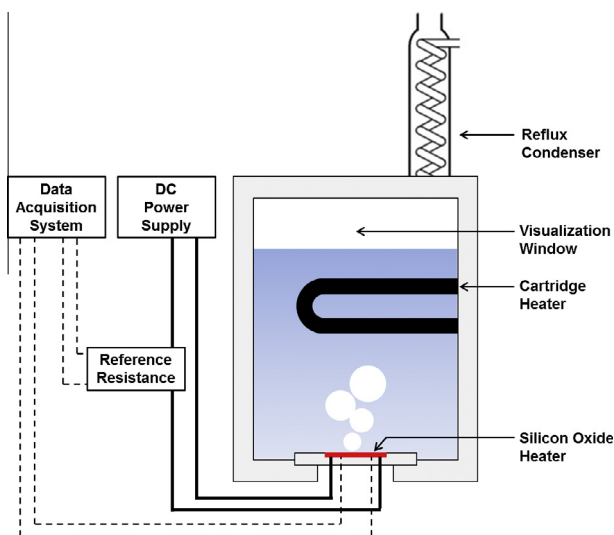


Fig. 1. Schematic diagram of the pool boiling experimental facility.

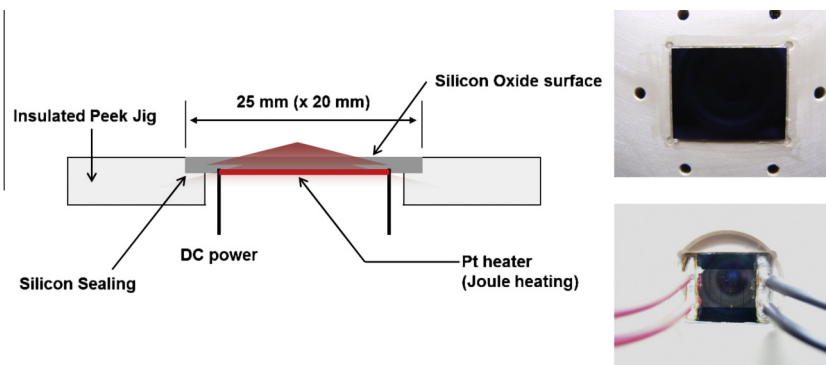


Fig. 2. Test heater (SiO<sub>2</sub> substrate and platinum film heater).

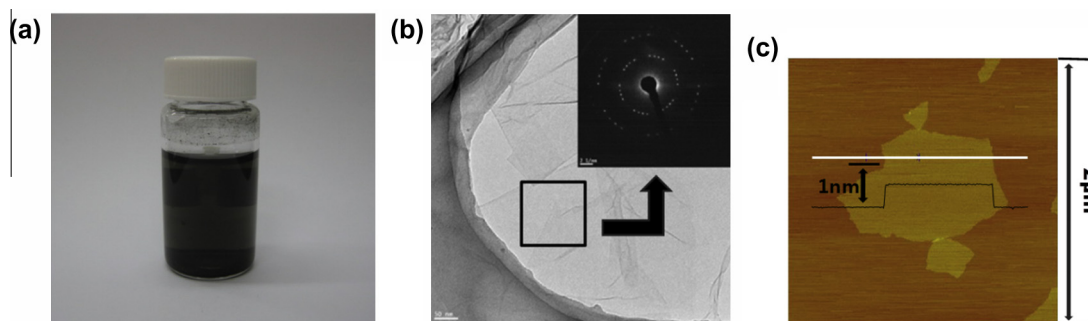


Fig. 3. Characteristics of the RGO colloid. (a) Optical image of the RGO colloid, (b) TEM image of an RGO flake (inset: SEAD image), (c) AFM image of an RGO flake.

performed over the area indicated by the box in the TEM image. The region was oriented along the [001] zone axis. The 24 spots in the first ring, corresponding to reflections from the (1100) plane, revealed hexagonal symmetry in the [0001] diffraction pattern [18]. These 24 bright spots represent four highly crystalline sheets of graphene that were overlapped. The thickness and size of the suspended RGO flakes in water, characterized via atomic force microscopy (AFM) measurements, were 0.675 nm and 0.5–1.0 μm, respectively. This was in agreement with RGO samples prepared by other processes [17,19], but exceeded that of a single graphene layer (0.334 nm). The apparent increase in the height of the graphene on mica was caused by residual epoxy and carbonyl groups that had not been fully reduced. Water-based RGO colloids were prepared at concentrations of 0.0005 wt.%.

### 3. Experimental results and discussion

#### 3.1. Boiling heat transfer characteristics in the RGO colloids boiling

RGO colloids were prepared at concentrations of 0.0005 wt.%. Fig. 4 shows the boiling curves for the RGO colloid and water, and indicates that the boiling heat transfer (BHT) the critical heat flux (CHF) were enhanced. In our previous studies [20–23], the base graphene layer (BGL) during RGO colloid boiling was formed near onset of nucleate boiling (ONB) on the heater surface. According to Ahn et al. [19,20], the RGO flakes were orderly stacked and horizontally aligned, finally formed the BGL with the thickness of 10–100 nm. Fig. 5 shows the transparent electron microscope (TEM) image of BGL, which could be confirmed that the well-aligned RGO flakes with the high magnitude at the side-view of BGL. After RGO colloid boiling, the RGO flakes provide the BGL and the self-assembled foam-like graphene (SFG) as regarding to Fig. 6. From our previous study, the mechanisms of BGL and SFG

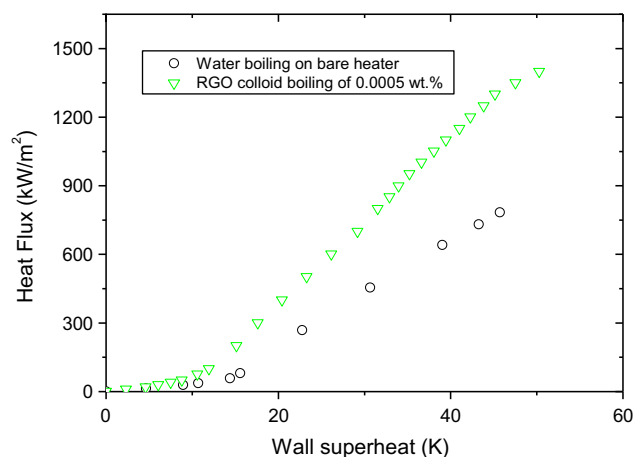


Fig. 4. Boiling curve of RGO colloid and water.

formation during the nucleate boiling were revealed such as the triple line movement during the bubble growth and the coalescence of bubbles during the bubble departure, respectively. The enhanced boiling heat transfer could be explained by the nano-scale cavity over the BGL and the less wettable surface. According to Ahn et al. [21], the contact angle of water droplet was 66° on silicon (bare) surface, however it was near 80° on BGL surface. Thus, the early enhanced BHT in RGO colloid boiling could be explained. Finally, According to Ahn et al., [21] why the CHF increase in RGO colloid boiling was supposed that the continuous nucleate boiling induced the surface deposition of RGO flakes, and the numerous nucleate boiling with lots coalescence of bubbles finally provided the SFG formation. The SFG leads the water absorption, nevertheless shows the hydrophobic property with the water droplet. In addition, the thermal activity of well-stacked graphene such like

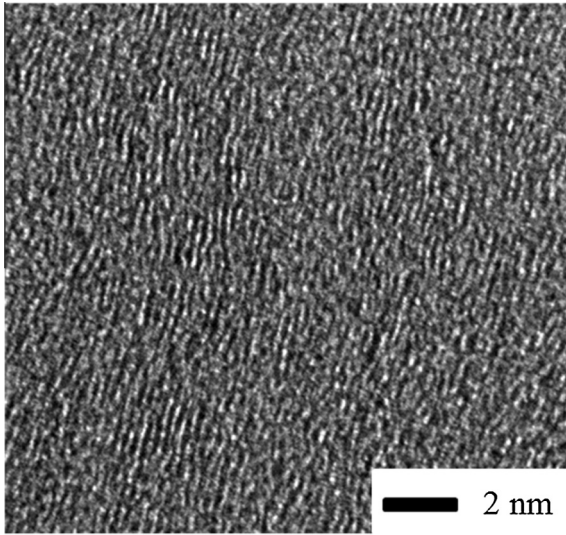


Fig. 5. TEM image of BGL.

BGL could play a role with dissipating the dry patch formation during the nucleate boiling, finally delay to trigger the CHF occurrence [22,23]. Recently, our research group reported that the heat dissipation on only BGL layer was more vigorous than it on bare surface using infrared high speed visualization, thus the CHF could be increased by the effective heat dissipation.

### 3.2. Boiling heat transfer characteristics on RGO film (water boiling)

In order to confirm the role of BGL (base graphene layer) on boiling heat transfer, we suggested an idea to make an artificial BGL, which could be same feature such as multilayered graphene films. As shown in Fig. 7, the filtration method was used to make the RGO films. The RGO colloid of 0.0001 wt.% was prepared as previously described in Section 2.3. Then, the RGO colloid was filtrated to prepare the graphene film of which the thickness was controlled by the following equation.

$$\delta = \frac{V_{colloid} \rho_{colloid}}{A \rho_{graphite}} \quad (2)$$

where  $V_{colloid}$ ,  $A$ ,  $\delta$ ,  $\rho_{graphite}$  and  $\rho_{colloid}$  are the volume of RGO solution, film area, film thickness, density of graphite and density of RGO solution. The cellulose membrane filter with 450 nm was used for the filtration. The graphene film was transferred to the bare heater surface as shown in Fig. 8. The filtrated graphene film was attached on the silicon heater surface with the compression. After drying process in the vacuum oven at 63 °C during 1 h, the filtration paper was taken out from the heater surface. The predicted thickness of graphene film was controlled to 50 nm, because the BGL thickness provided by the nucleate boiling was 10–100 nm. After transfer process, the water boiling experiment was conducted on the RGO film coated surface. As shown in Fig. 9, the boiling curves of water boiling on bare and RGO films coated surfaces shows the different boiling characteristics. The

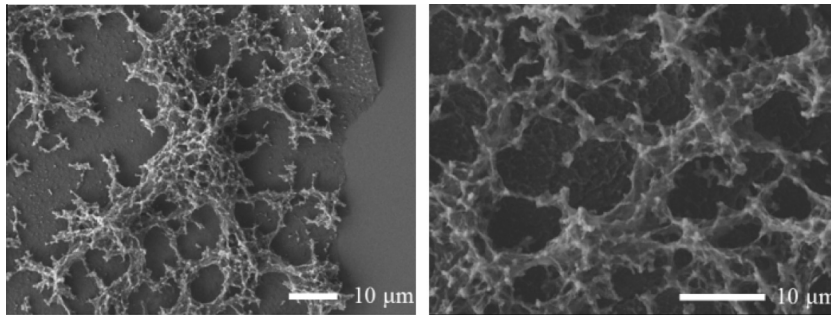


Fig. 6. Surface deposition of RGO flakes (BGL and SFG).

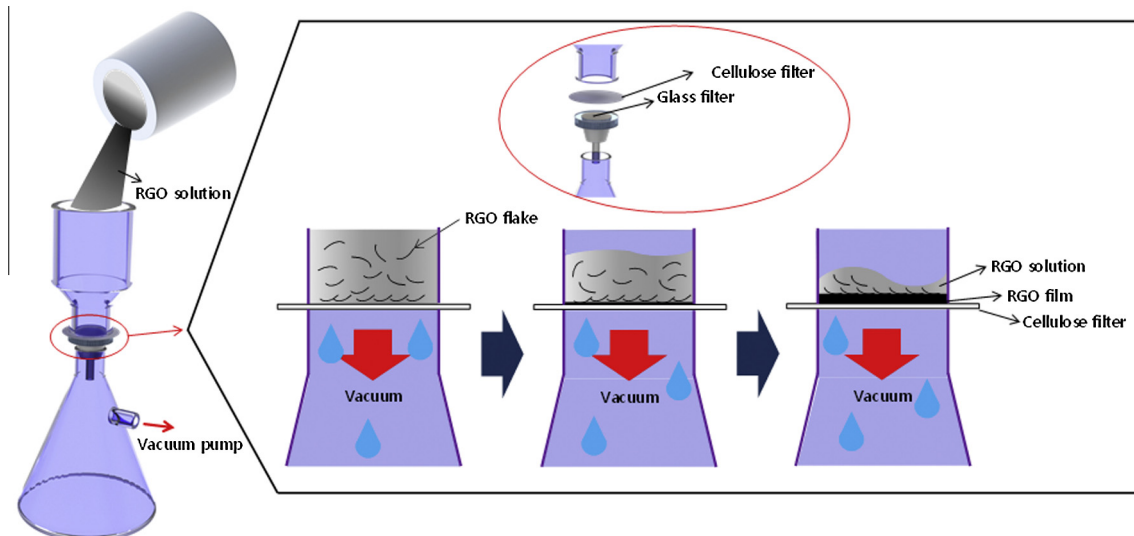


Fig. 7. Filtration of RGO colloid.

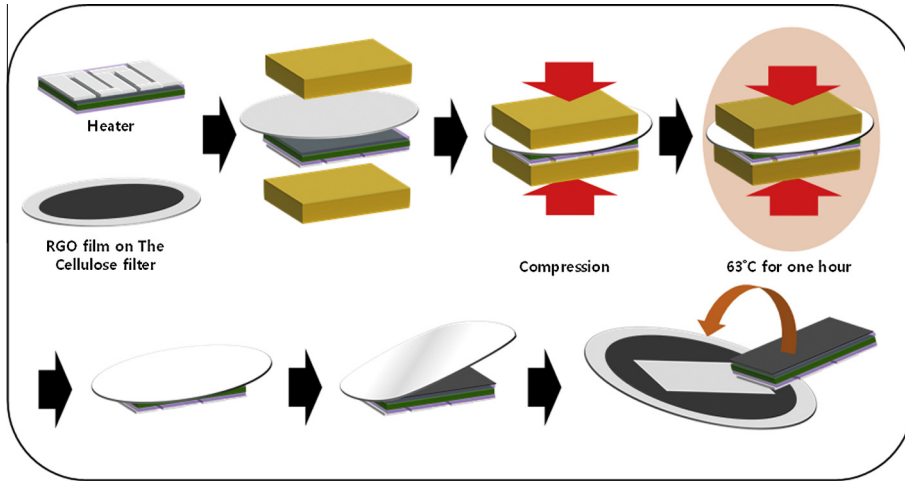


Fig. 8. RGO film transfer method.

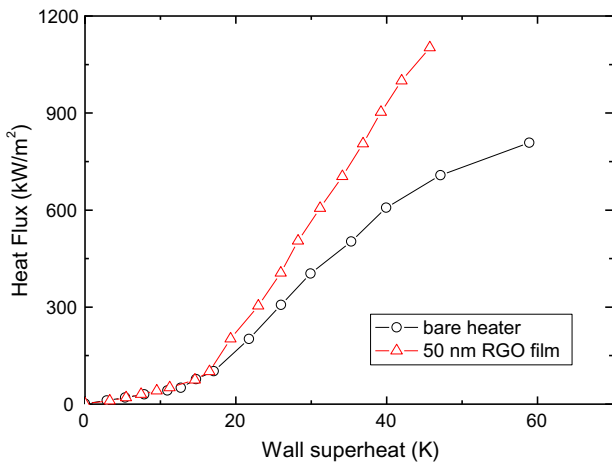


Fig. 9. Boiling curve of water boiling on bare and RGO film coated heaters.

case of RGO films coated surface shows the enhanced boiling heat transfer (BHT) and critical heat flux (CHF). In the previous section,

the RGO colloid boiling shows the better BHT (max. 65%) and CHF (70%) than the water boiling. As similar with RGO colloid boiling, the water boiling on the RGO films coated surface shows the better BHT (42%) and CHF (60%) than the water boiling on the bare surface. Fig. 10 shows the SEM images of BGL layers (side view) and the RGO film (artificially filtrated RGO layer) which are nearly same features. In addition, the contact angle of water droplet on the RGO film coated heater shows a similar characteristics as shown in Fig. 11. From comparison with the boiling and surface characteristics of RGO colloid boiling on bare heater and water boiling on RGO film coated heater, the enhanced BHT and CHF in RGO colloid boiling could be explained by mainly BGL formation near the ONB: In detail, the enhanced thermal effusivity by the high thermal conductivity of RGO flakes could be a reason to increase the boiling performance. Second, the nano-scaled cavities on the BGL and the RGO films could be a reason to increase the boiling performance, because lots bubble generations and its heat removal ability could induce to delay the hot/dry spot formation before CHF occurs. As similar to the earlier description about CHF increase, the RGO film could dissipate a heat during boiling like a BGL in RGO colloid boiling.

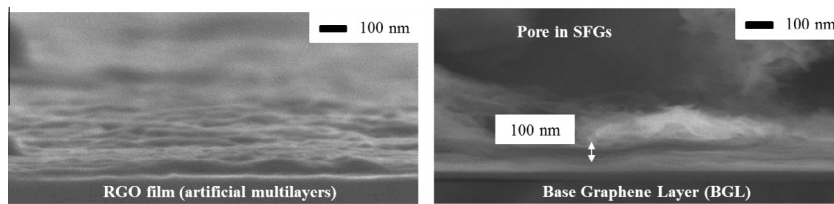


Fig. 10. SEM images of RGO film and BGL (side-view).

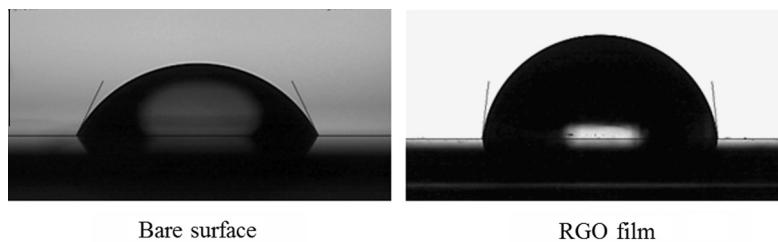


Fig. 11. Contact angle measurement on bare heater, RGO film coated heater.

#### 4. Conclusions

In this paper, we introduced our recent results of boiling performance using the graphene (reduced graphene oxide: RGO) as the heater and the working fluid. First, we conducted water and RGO colloid boiling. The boiling heat transfer (BHT) and critical heat flux (CHF) were increased as 65% and 70%, respectively. Second, we conducted the water boiling experiment (until CHF) on bare and RGO film coated heater. The boiling performance and CHF on RGO film coated heater increased more than those on bare heater. It also showed the similar result with the boiling performance of RGO film coated heater.

#### Acknowledgments

This work was supported by the National Research Foundation of Korea (NRF) grant funded by the Korea government (MEST) (2012R1A1A2002900). This work was supported by the Incheon National University (International Cooperative) Research Grant in 2013.

#### Appendix A

Prior to the boiling experiments, the working fluid was heated in the pool for 1 h via a submerged cartridge heater for degassing purposes. During the experiments, the heat flux was increased in 100-kW/m<sup>2</sup> steps after 2 min for steady-state data gathering. At heat fluxes less than 100 kW/m<sup>2</sup>, a 10-kW/m<sup>2</sup> step was used to observe the onset of nucleate boiling (ONB). When the CHF occurred during water boiling, the wall temperature increased rapidly, and the electric power was immediately shut down to prevent heater failure.

The analysis of the experimental uncertainty was based on the work of Holman [15]. Using our experimental data, the general formula for heat flux calculation is

$$q'' = \frac{V_{heater} \cdot V_{ref}}{R_{ref} \cdot A_{heater}} \quad (3)$$

The functional form of Eq. (3) is

$$q'' = q''(V_{heater}, V_{ref}, R_{ref}, A_{heater}), \quad (4)$$

where  $A_{heater}$  is assumed to be constant. The uncertainty analysis expression becomes

$$U_{q''}^2 = \left( \frac{\partial q''}{\partial V_{heater}} \right)^2 U_{V_{heater}}^2 + \left( \frac{\partial q''}{\partial V_{ref}} \right)^2 U_{V_{ref}}^2 + \left( \frac{\partial q''}{\partial R_{ref}} \right)^2 U_{R_{ref}}^2 \quad (5)$$

where  $U_{q''}$ ,  $U_{V_{heater}}$ ,  $U_{V_{ref}}$ , and  $U_{R_{ref}}$  represent the uncertainties in  $q''$ ,  $V_{heater}$ ,  $V_{ref}$ , and  $R_{ref}$ , respectively. Eq. (5) can be simplified to

$$\frac{U_{q''}}{q''} = \sqrt{\frac{U_{V_{heater}}^2}{V_{heater}^2} + \frac{U_{V_{ref}}^2}{V_{ref}^2} + \frac{U_{R_{ref}}^2}{R_{ref}^2}} \quad (6)$$

The uncertainty of the heater surface temperature was also calculated. The general form of the relationship for surface temperature is

$$T_{wall} = \frac{1}{a} (R_{heater}) = \frac{1}{a} \left( \frac{V_{heater} \cdot R_{ref}}{V_{ref}} \right) \quad (7)$$

The general expression for the uncertainty of the surface temperature is

$$\frac{U_{wall}}{\Delta T_{wall}} = \sqrt{\frac{U_{V_{heater}}^2}{V_{heater}^2} + \frac{U_{V_{ref}}^2}{V_{ref}^2} + \frac{U_{R_{ref}}^2}{R_{ref}^2}} \quad (8)$$

Accounting for all instrument errors, the maximum uncertainties of the heat flux and wall temperature were estimated to be less than 1.8% and 3.0%, respectively, over the expected CHF range.

#### References

- [1] H.D. Kim, J.B. Kim, M.H. Kim, Effect of nanoparticles on CHF enhancement in pool boiling of nano-fluids, *Int. J. Heat Mass Transf.* 49 (25–26) (2006) 5070–5074.
- [2] H.S. Ahn, H.J. Jo, S.H. Kang, M.H. Kim, Effect of liquid spreading due to nano/microstructures on the critical heat flux during pool boiling, *Appl. Phys. Lett.* 98 (2011) 071908.
- [3] H.S. Ahn, C. Lee, J. Kim, M.H. Kim, The effect of capillary wicking action of micro/nano structures on pool boiling critical heat flux, *Int. J. Heat Mass Transf.* 55 (2012) 89–92.
- [4] H.D. Kim, M.H. Kim, Effect of nanoparticle deposition on capillary wicking that influences the critical heat flux in nanofluids, *Appl. Phys. Lett.* 91 (1) (2007) 014104.
- [5] M.N. Golubovic, H.D. Madhawa Hettiarachchi, W.M. Worek, W.J. Minkowycz, Nanofluids and critical heat flux, experimental and analytical study, *Appl. Therm. Eng.* 29 (2009) 1281–1288.
- [6] S.K. Das, N. Putra, W. Roetzel, Pool boiling characteristics of nano-fluids, *Int. J. Heat Mass Transf.* 46 (2003) 851–862.
- [7] H.S. Ahn, G. Park, J.M. Kim, M.H. Kim, Visualized effect of alumina nanoparticles surface deposition on water flow boiling heat transfer, *Exp. Thermal Fluid Sci.* 37 (2012) 154–163.
- [8] S.M. Kwark, R. Kumar, G. Moreno, J. Yoo, S.M. You, Pool boiling characteristics of low concentration nanofluids, *Int. J. Heat Mass Transf.* 53 (5–6) (2010) 972–981.
- [9] A.A. Balandin, S. Ghosh, W. Bao, I. Calizo, D. Teweldebrhan, F. Miao, C.N. Lau, Superior thermal conductivity of single-layer graphene, *Nano Lett.* 8 (3) (2008) 902–907.
- [10] K.S. Novoselov, A.K. Geim, S.V. Morozov, D. Jiang, M.I. Katsnelson, I.V. Grigorieva, S.V. Dubonos, A.A. Firsov, Two-dimensional gas of massless Dirac fermions in graphene, *Nature* 438 (2005) 197–200.
- [11] K.S. Novoselov, A.K. Geim, S.V. Morozov, D. Jiang, Y. Zhang, S.V. Dubonos, I.V. Grigorieva, A.A. Firsov, Electric field effect in atomically thin carbon films, *Science* 306 (2004) 666–669.
- [12] C. Lee, X.D. Wei, J.W. Kysar, J. Hone, Measurement of the elastic properties and intrinsic strength of monolayer graphene, *Science* 321 (2008) 385–388.
- [13] S. Youngchao, T.S. Edward, Synthesis of water soluble graphene, *Nano Lett.* 8 (2008) 1679–1682.
- [14] W. Jang, Z. Chen, W. Bao, C.N. Lau, C. Dames, Thickness-dependent thermal conductivity of encased graphene and ultrathin graphite, *Nano Lett.* 10 (10) (2010) 3909–3913.
- [15] J.P. Holman, *Experimental Methods for Engineers*, seventh ed., McGraw-Hill, New York, 2001. Chapter 3.
- [16] H.J. Jo, H.S. Ahn, S.H. Kang, M.H. Kim, A study of nucleate boiling heat transfer on hydrophilic, hydrophobic and heterogeneous wetting surfaces, *Int. J. Heat Mass Transf.* 54 (2011) 5643–5652.
- [17] W.S. Hummers, R.E. Offeman, Preparation of graphitic oxide, *J. Am. Chem. Soc.* 80 (6) (1958) 1339.
- [18] D. Li, M.B. Müller, S. Gilje, R.B. Kaner, Processable aqueous dispersions of graphene nanosheets, *Nat. Nanotechnol.* 3 (2008) 101–105.
- [19] H.S. Ahn, J.-W. Jang, M. Seol, J.M. Kim, D.-J. Yun, C. Park, H. Kim, D.H. Youn, J.Y. Kim, G. Park, S.C. Park, J.M. Kim, D.I. Yu, K. Yong, M.H. Kim, J.S. Lee, Self-assembled foam-like graphene networks formed through nucleate boiling, *Sci. Rep.* 3 (2013) 1396.
- [20] H.S. Ahn, J.M. Kim, C. Park, J.-W. Jang, J.S. Lee, H. Kim, M. Kaviany, M.H. Kim, A novel role of three dimensional graphene foam to prevent heater failure during boiling, *Sci. Rep.* 3 (2013) 1960.
- [21] H.S. Ahn, H. Kim, J.M. Kim, S.C. Park, J.M. Kim, J. Kim, M.H. Kim, Controllable pore size of three dimensional self-assemble foam-like graphene and its wettability, *Carbon* 64 (2013) 27–34.
- [22] H.S. Ahn, J.M. Kim, M.H. Kim, Pool boiling experiments in reduced graphene oxide colloid. Part 1 – boiling characteristics, <<http://dx.doi.org/10.1016/j.ijheatmasstransfer.2014.01.022>>.
- [23] H.S. Ahn, J.M. Kim, M.H. Kim, Pool Boiling Experiments in Reduced Graphene Oxide Colloids Part II – Behavior after the CHF, and Boiling Hysteresis, *Int. J. Heat Mass Tran.* (2014). in press.